Phase behavior of liquid crystals confined to controlled porous glass studied by deuteron NMR

S. Kralj,[1,2,3] A. Zidanšek,[1] G. Lahajnar,[1] S. Žumer,[1,2] and R. Blinc[1,2]
[1]*J. Stefan Institute, University of Ljubljana, Jamova 39, 1000 Ljubljana, Slovenia*
[2]*Department of Physics, FMF, University of Ljubljana, Jadranska 19, 1000 Ljubljana, Slovenia*
[3]*Department of Physics, Faculty of Education, University of Maribor, Koroška 160, 2000 Maribor, Slovenia*
(Received 20 October 1997)

The phase behavior of pentylcyanobiphenyl (5CB) and octylcyanobiphenyl (8CB) liquid crystals confined to controlled porous glass of different characteristic void sizes R is studied using deuteron NMR. In samples with the 5CB liquid crystal the discontinuous isotropic-nematic (I-N) transition becomes gradual for $R < 0.025\ \mu$m. The discontinuous I-N phase transition temperature shift ΔT_{IN} scales as $\Delta T_{IN} \propto R^{-1.3\pm0.3}$. A detailed theoretical analysis of the origins of the temperature shift and the change of the character of the I-N and nematic–smectic-A phase transition is given. The influence of the surface treatment is studied for the 8CB liquid crystal immersed in a $R = 0.2\ \mu$m matrix. The results suggest that for the silane-treated sample the anchoring is homeotropic, whereas it is planar for the nontreated surface. In both cases the corresponding anchoring strength is estimated to be larger than 10^{-5} J/m^2. The smectic-A ordering seems to be more affected by the confinement in the nontreated sample than the one treated by silane. [S1063-651X(98)01303-8]

PACS number(s): 64.70.Md, 76.60.−k

I. INTRODUCTION

In recent years there has been a growing interest in the physics of porous materials [1]. These systems play an increasingly important role in various technological applications (e.g., nuclear waste storage, separation, oil recovery, heterogeneous catalysis, glass processing, thermal insulation of refrigerators, and passive solar energy collection devices). In addition, they provide model systems for the study of several fundamental problems in physics. In a number of such studies porous matrices serve as a rigid host frame for various fluids. It is advantageous that the immersed fluid is close to a phase transition where its susceptibility to various perturbations is anomalously increased. From the changes of the physical behavior of the confined fluid induced by the porous matrix one can infer information about the enclosing surface, finite-size effects, random field, random bond phenomena, etc.

As a confined fluid various liquid crystals (LCs) are particularly useful. The reason for this is that (i) they exhibit a variety of phases with different degrees of orientational or translational order, (ii) there exist different kinds of transitions between these phases (e.g., first- and second-order phase transitions in orientational or translational degrees of order), (iii) they are typical representatives of soft materials (their response to perturbations induced by the confining matrix is pronounced and long ranged), (iv) LCs and the host matrix do not interact chemically, and (v) both LCs and the host matrix are in most cases transparent and consequently samples can be studied using a variety of optical methods. The phase and the structure of the confined LC reflects the competition among the LC elastic, surface, and external field forces. Their relative strength strongly depends upon the value of the typical size R characterizing a confining cavity.

As porous material Anopore [2,3] and Nuclepore [4] membranes, controlled porous glass [5–7] (CPG), Vycor glass [8,9], aerogels [10–13], or similar porous glasses [14,15] are conventionally used. In Anopore and Nuclepore materials the voids can be described as long, straight noninterconnected cylinders. In CPG the voids are also cylindrically shaped, but are strongly curved and interconnected. Anopore, Nuclepore, and CPG matrices have a relatively narrow distribution of pore sizes. The structure of the Vycor glass is reminiscent of that of the CPG, but with relatively large local departures from the cylindrical geometry. In aerogels the voids are separated by randomly interconnected silica strands forming the matrix. Consequently, the geometry of voids is strongly irregular. In these systems the degree of randomness increases from Anopore to aerogels. In all matrices the characteristic size of voids is typically below the micrometer range (for some matrices even in the nanometer range).

The most important results inferred from studies of LCs immersed in various porous materials are the following. (i) Even at temperatures far above the bulk isotropic-nematic (I-N) phase transition there exists a weak residual nematic ordering at the enclosing surface. Consequently, it is often more appropriate to call the corresponding phase paranematic rather than isotropic. (ii) The isotropic-nematic transition seems to be gradual for porous matrices with characteristic cavity sizes below 0.1 μm. (iii) The nematic–smectic-A (N–Sm-A) phase transition is usually more affected by confinement than the I-N one. (iv) An additional slow relaxation mechanism is observed in confined samples that is not observed in the bulk. Most of these topics are not yet completely understood. In particular, it is not yet clear in which of the last three phenomena listed randomness [16–19], introduced into the LC system via the geometry of a confining porous matrix, plays a significant role.

In order to resolve these problems a systematic study of various porous matrices and LCs is needed. For this reason we performed a deuteron NMR study on the pentylcyanobiphenyl (5CB) and octylcyanobiphenyl (8CB) liquid crystals immersed in various CPG matrices. We study the LC phase behavior as a function of temperature, typical void size R, and surface treatment of the CPG voids. The study comple-

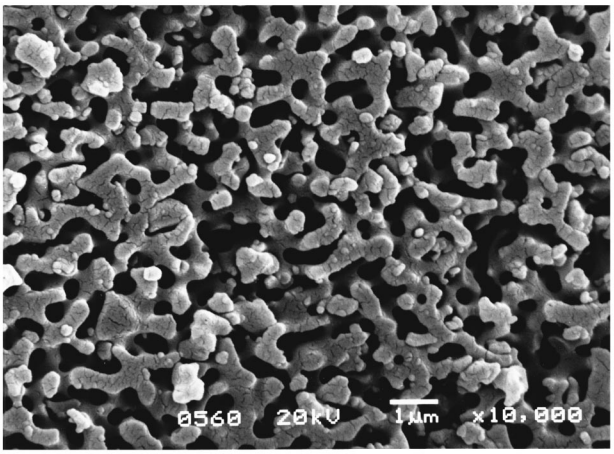

FIG. 1. SEM photograph of a CPG matrix with $R=0.2\ \mu$m.

ments our previous publication [6] in this field where we focused on the line shape of the deuteron absorption spectra and qualitatively discussed the possible origins of the gradual I-N transition and the hysteresis phenomena observed.

The structure of this article is as follows. In Sec. II the experimental setup and experimental results are presented. The theoretical basis used in the explanation of the experimental data is given in Sec. III and the free energy of the model is introduced. The corresponding temperature shifts of the I-N and $N-$Sm-A phase transition of a LC confined to a cavity of arbitrary shape are evaluated and their dependence on the cavity size is analyzed. In Sec. IV we introduce model structures that imitate the most important characteristics of the CPG samples In Sec. V the theoretical results are discussed. In Sec. VI the conclusions are summarized.

II. EXPERIMENT

A. Experimental setup

We studied 5CB and 8CB liquid crystals confined to CPG matrices with average pore diameters $2R=7.4$, 24, 50, 100, 140, 300, and 400 nm. The CPG matrices have a narrow monodispersed pore diameter distribution with $5-10\%$ departures around the average value. The surface of the voids is smooth down to the nanometer scale [6]. A typical scanning electron microscopy (SEM) photograph of a CPG matrix is shown in Fig. 1. The internal pore surface was either nontreated or treated with silane. The immersed 5CB and 8CB LCs were deuterated at the β-d_2 and α-d_2 positions, respectively. Deuteron NMR spectra were recorded at the resonance frequencies of 58.37 and 30.6 MHz. A $(\pi/2)_x-(\pi/2)_y$ solid echo pulse sequence with phase cycling was used to obtain the absorption spectra.

B. Determination of the LC ordering

In our experiment the degree of LC ordering was inferred from the deuteron NMR absorption spectrum. The details are described in Ref. [6]. Here we just summarize the main facts.

The shape of the absorption spectrum $I(\nu)$ can in general reveal the nematic ordering and yield information about the translational diffusion of LC molecules. If a nematic phase exhibits predominantly uniaxial character, which is often realized, the nematic ordering is well described [20] in terms of the nematic director field $\mathbf{n}(\mathbf{r})$ and the orientational order parameter $S(\mathbf{r})$. A nematic molecule fixed at $\mathbf{r}$ and oriented along $\mathbf{n}$ contributes to $I(\nu)$ two lines separated by [21] $2\Delta\nu$, where

$$\Delta\nu(\vec{r})=\Delta\nu_0 S(\vec{r})\left(\frac{3[\vec{n}(\vec{r})\cdot\vec{e}_f]^2-1}{2}\right). \tag{1}$$

The unit vector $\mathbf{e}_f$ points along the external magnetic field $\mathbf{B}$ used in the NMR experiment. $\Delta\nu_0$ describes the half splitting of lines for a perfectly aligned (i.e., $S=1$) nematic molecule. A typical value of the half splitting in the bulk N phase is $S\Delta\nu_0\approx 20$ kHz for 5CB and $S\Delta\nu_0\approx 30$ kHz for 8CB LCs, where S describes the average degree of nematic ordering. The spectrum of the whole sample consists of a superposition of such contributions from all molecules. The sample of a homogeneously aligned nematic again consists of two lines. Departures from this shape reveal the spatial variation of the nematic ordering. For example, $I(\nu)$ is powder shaped in case that (i) all orientation of $\mathbf{n}$ are equally occupied, (ii) $S(\mathbf{r})$ is spatially homogeneous, and (iii) the translational diffusion is not effective. Condition (i) is, in our experiment, enforced by the geometry of the CPG sample.

If, however, the external NMR magnetic field is strong enough (which is realized for $R/\xi_f>1$, where ξ_f is the external magnetic-field correlation length [20]), the $\mathbf{n}$ distribution becomes strongly anisotropic. On average more molecules are oriented along $\mathbf{e}_f$ and consequently the external wings of $l(\nu)$ are more pronounced. For the $B\approx 9$ V s/m^2 used in our experiment it follows that $\xi_f\approx 0.5\ \mu$m. Thus, in the samples with $R>0.1\ \mu$m the external field influence is expected to be already observable.

Because of the translational diffusion nematic molecules diffuse for an average distance [22] $d\cong\sqrt{\langle D\rangle/(\Delta\nu_0 S)}$ during the NMR acquisition time. Here $\langle D\rangle$ is the average translational diffusion constant. For 5CB and 8CB one typically finds $d\approx 0.01\ \mu$m in the nematic phase. Since in most cases the director field deformations extend on the scale given by R, one expects that the effect of motional averaging is negligible in samples where the condition $R\gg d$ is realized. In our study the diffusion effect is discarded.

Although the shape of the absorption spectra is directly related to the degree of nematic ordering, it can also give indirect information on the smectic-A ordering. In the smectic-A phase the LC molecules are forced to align along the layer normal. Consequently, the degree of the nematic ordering is increased (i.e., in the N phase orientational fluctuations are Goldstone modes that cost little energy, in contrast, in the Sm-A phase, such fluctuations change the layer spacing and represent hard modes).

C. Results

In the experiment we have focused on the (i) dependence of the I-N phase transition on R, (ii) the influence of the surface treatment on the nematic and Sm-A phase ordering, and (iii) the effect of the external field reorientation on $I(\nu)$. The investigation (i) was performed on 5CB and the studies (ii) and (iii) on 8CB LCs.

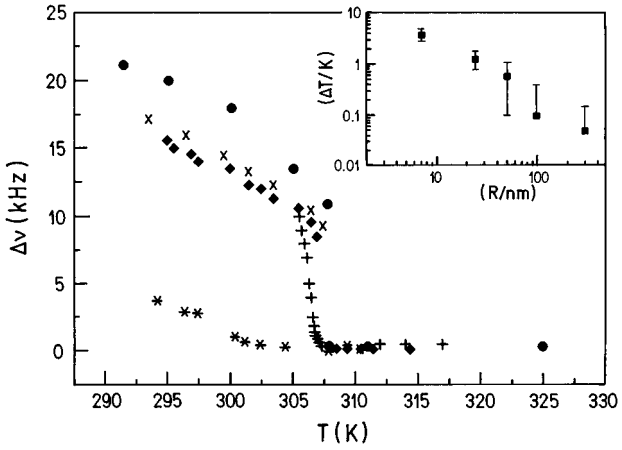

FIG. 2. Temperature dependence of the deuteron NMR half splitting $\delta\nu$ for various R for the 5CB liquid crystal in nontreated CPG matrices. Shown in the inset is the I-N phase temperature shift as a function of R. $2R=7.4$ nm (*), $2R=24$ nm, (+), $2R=50$ nm (♦), $2R=100$ nm (×), and $2R=140$ nm (●).

In Fig. 2 the temperature dependence of the absorption spectra width $\Delta\nu$ as a function of R is shown. The measured spectra can be roughly assigned according to their shape into three qualitatively very different groups: powder shapelike, fieldlike, and single peaklike spectra. The powder shapelike spectra resemble the ''ideal'' powder shaped spectra characteristic for an isotropic **n** distribution and a spatially homogeneous value of S. In the fieldlike spectra the external wings are dominant, revealing the strong influence of the external magnetic field. The single peaklike spectra consist of a single peak. Details about the shape of spectra and related hysteresis phenomena were discussed in Ref. [6]. The $\Delta\nu=\Delta\nu(T,R)$ dependence suggests that in samples with $R<0.025$ μm the I-N transition is gradual, whereas it is discontinuous for $R\geqslant 0.025$ μm. In the inset the dependence of the decrease of the I–N phase transition temperature $\Delta T_{IN}(R)$ on R is shown.

The influence of the surface treatment on the nematic and smectic-A ordering was studied in the 8CB LC confined to the CPG matrix characterized by $R=0.2$ μm. The internal CPG surface was either nontreated or treated with silane. The spectra measured show a remarkable dependence on the surface treatment, as shown in Fig. 3. The spectra are powder shapelike in the treated and fieldlike in the nontreated case. In this figure the influence of $I(\nu)$ on the sample reorientation with respect to the external field is also shown. For this purpose the LC was cooled in the external field from the isotropic phase deeply into the nematic phase. Then the sample was reoriented for an angle θ_1 with respect to the external field and the absorption spectrum was measured. The time interval $\Delta\tau=\tau_2-\tau_1$ between the time τ_1, when the sample was reoriented, and the time τ_2, when the $I(\nu)$ measurement was performed, was long enough so that the structural changes in the sample were already ''saturated.'' We used $\Delta\tau\approx 15$ min. In Fig. 3 the sequence for $\theta_f=0°-90°$ is shown for the (a) treated and (b) nontreated samples. In this cycle a weak hysteresis effect is observed. It is larger in the nontreated case. The spectra also indicate that the director field structure is, to a great extent, locked in the initial state. Thus the surface interaction is strong enough to conserve the initial state established before the rotation of the sample is performed.

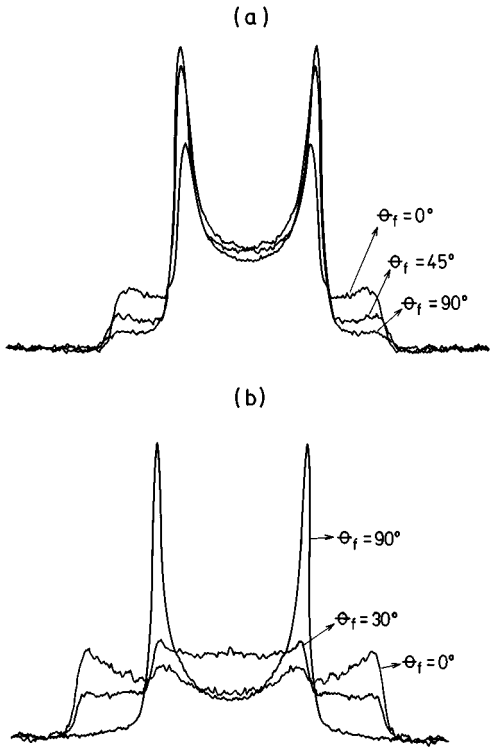

FIG. 3. Deuteron NMR absorption spectra for the (a) silane-treated and (b) nontreated sample for different angles θ_f. $R=0.2$ μm for the 8CB LC.

Next we focus our interest on the effect of the surface treatment on the N–Sm-A phase transition. The bulk 8CB LC exhibits in the temperature interval studied the isotropic, nematic, and Sm-A phases. The temperature evolution $\Delta\nu=\Delta\nu(T)$ for the treated, nontreated, and bulk sample is shown in Fig. 4. The N–Sm-A transition is clearly observable in the bulk sample because of the coupling between the nematic and smectic order parameters. The coupling causes a sudden anomalous increase in $\Delta\nu(T)$ observed at $T\approx 309$ K. The results indicate that due to the confinement,

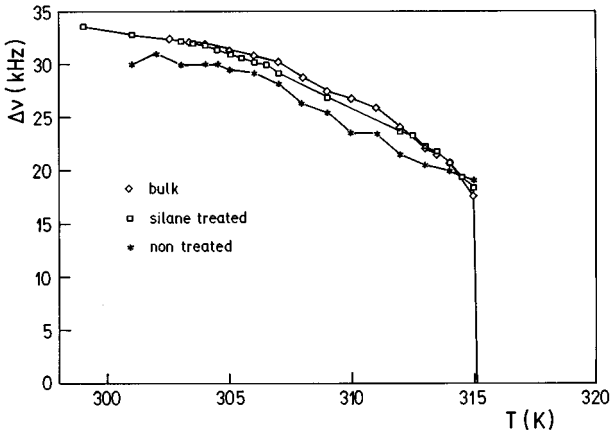

FIG. 4. Temperature dependence of $\delta\nu$ for the 8CB LC confined to the silane-treated and nontreated CPG matrix. For comparison the bulk dependence is also shown. $R=0.2$ μm.

the $N-$Sm-A phase transition is less pronounced only in the nontreated sample.

III. THEORY

A. Free energy

In the following phenomenological model the phase and the structure of the enclosed liquid crystal are described with the nematic director field **n**, the nematic orientational order parameter S, and the smectic complex order parameter $\psi = \eta e^{i\Phi}$. The quantity η is the smectic translational order parameter and Φ the phase factor determining the position of smectic layers. The corresponding free energy F is expressed as [20,23–25]

$$F=\int \left(A_0(T-T_*)S^2 - bS^3 + cS^4 + \frac{K_{11}}{2}(\mathrm{div}\vec{n})^2 + \frac{K_{22}}{2} \times(\vec{n}\times\mathrm{curl}\vec{n})^2 + \frac{K_{33}}{2}(\vec{n}\cdot\mathrm{curl}\vec{n})^2 + \frac{L}{2}(\mathrm{grad}S)^2 - \frac{K_{24}}{2}\mathrm{div}(\vec{n}\times\mathrm{curl}\vec{n}+\vec{n}\cdot\mathrm{div}\vec{n}) - \frac{\Delta\chi S B^2}{2\mu_0}(\vec{n}\cdot\vec{e}_f)^2 + \alpha_0(T-T_{NA})|\Psi|^2 + \frac{\beta}{2}|\Psi|^4 - DS|\Psi|^2 + C_\parallel|(\vec{n}\cdot\mathrm{grad}-q)\Psi|^2 + C_\perp|(\vec{n}\times\mathrm{grad})\Psi|^2 \right) d^3\vec{r} + \int (f_n+f_s)d^2\vec{r}. \quad (2)$$

The elastic properties of the enclosed LC are described by the nematic $(L,K_{11},K_{22},K_{33},K_{24})$ and the smectic $(C_\parallel,C_\perp)$ elastic constants. The strength of the coupling between the nematic and the smectic order parameter is given by the coupling [20] constant D. The saddle splay term [20,26,27] weighted by the elastic constant K_{24} can be transformed to the surface enclosing the nematic phase using the Gauss theorem. We have discarded the so-called K_{13} contribution [28,29]. All the listed nematic elastic constants are temperature dependent, except the bare nematic elastic constant L. Their temperature dependence is conventionally expressed via the expansion [23] in S. The Frank elastic constants (K_{11},K_{22},K_{33}) are to the lowest order quadratic and the saddle splay elastic constant K_{24} is linear in S. Note that in Eq. (2) most of the terms including spatial derivatives [23] in S are discarded, except the term with the elastic constant L. These terms are not essential for our study because most of the calculations are performed in the approximation of a spatially constant nematic orientational order parameter. The smectic compressibility term tends to enforce the interlayer separation $d=2\pi/q$ if $\eta>0$. Quantities $A_0,b,c,\alpha_0,\beta,T_*,T_{NA}$ are the material constants and T is the temperature. In bulk the first-order I-N phase transition takes place at $T=T_{IN}=T_*+b^2/(4A_0c)$ and the second-order $N-$Sm-A phase transition at $T=T_{NA}$ for $D=0$. With an increasing value of D the $N-$Sm-A phase transition increases. Above the critical value $D=D_c$ the $N-$Sm-A transition becomes discontinuous [20]. In this work we consider only the case $D\ll D_c$. T_* is the nematic supercooling temperature. The quantity **B** is the external magnetic field pointing along the direction $\mathbf{e}_f$, $\Delta\chi$ is the magnetic anisotropy, and μ_0 is the magnetic influence constant. The LC-surface interaction is modeled by the nematic orientational (f_n) and the smectic positional (f_s) anchoring term.

In this study we model the nematic surface interaction by [30]

$$f_n=-W_1S\left(\frac{3(\vec{n}\cdot\vec{e})^2-1}{2}\right)+W_2S^2. \quad (3)$$

Here W_1 and W_2 are positive surface anchoring constants. The unit vector **e** is conventionally called the easy direction. If $\mathbf{n}=\mathbf{e}$ is realized at the surface the nematic orientational part of f_n is minimized. Molecular models [31,32] indicate that the origin of the linear term is the direct interaction between the surface and LC molecules and the S^2 term is due to the fact that LC molecules have fewer neighbors at the surface. The S^2 contribution is believed to be dominant at porous silica surfaces and evaporated surfaces.

The smectic positional anchoring can be modeled [33] by

$$f_s=-W_p\eta\cos(\Phi-\Phi_s), \quad (4)$$

where W_p is a positive constant. It tends to establish the layer variation described by Φ_s and promotes the Sm-A ordering.

For further convenience we rewrite Eq. (2) in the dimensionless form. For this purpose we scale distance in units of the characteristic cavity size R (in the case of a cylindrical cavity R denotes its radius) and introduce dimensionless operators $\vec{\nabla}\cdot=R$ div, $\vec{\nabla}\times=R$ curl, and $\vec{\nabla}=R$ grad. The order parameters are scaled as $S=sS_0$ and $\eta=\varepsilon\eta_0$, where $S_0=S(T=T_{NI})=b/2c$ and $\eta_0^2=\eta(T=0)^2=\alpha_0T_{NA}/\beta$. We next confine our interest to I-N and then to the $N-$Sm-A phase transition for a LC confined to a cavity characterized by a typical size R.

B. I-N phase transition

In order to gain qualitative insight into the temperature behavior at the isotropic-nematic phase transition in the CPG sample we apply the following approximations.

(i) The temperature dependence of the nematic elastic constants K_{ii} $(ii=11,22,33,24)$ is expanded [23] up to the second order in S. Because of the symmetry arguments, only the saddle splay constant has also a linear contribution [34].

(ii) Spatial variations in S are neglected everywhere but at the defects. At defects $S=0$ and $S(\mathbf{r})$ recovers its average value in the sample if the distance between a point **r** and the defect is larger than the nematic correlation length $\xi_n(T)$. In this study only point defects are relevant and the variation of S at a defect site is approximated by a linear dependence on the separation distance.

(iii) In the minimization procedure first the director field is expressed assuming a constant value of S. The resulting expression for the free energy is then minimized over S.

Taking these into account, the dimensionless free energy G of a LC in a cavity above the $N-$Sm-A phase transition is expressed as a simple expansion [12,19] in $s=S/S_0$:

$$G=t_n s^2-2s^3+s^4-h_n^2 s. \tag{5}$$

The parameters t_n and h_n play the role of the effective temperature and the effective external field, respectively, given by

$$t_n=\frac{T-T_*}{T_{IN}-T_*}+\left(\frac{\xi_n}{R}\right)^2(a_0 G_e-a_2 G_{24})+\frac{\xi_n^2}{d_2 R}+t_{\rm def}, \tag{6a}$$

$$h_n^2=\left(\frac{\xi_n}{R}\right)^2 a_1 G_{24}+\frac{\xi_n^2}{d_1 R}\,G_n+\left(\frac{\xi_n}{\xi_f}\right)^2 G_f. \tag{6b}$$

The ratios of the nematic elastic constants a_i $(i=0,1,2)$ are expressed at $T=T_{IN}$ and are typically of order one: $a_0=K_{11}(T_{IN})/LS_0^2$, $a_1=k_1 S_0/LS_0^2$, and $a_2=k_2/L$, where $K_{24}=k_1 S+k_2 S^2$. ξ_n describes the nematic correlation length [20], ξ_f is the external magnetic-field correlation length [20], and d_1, d_2 are the surface extrapolation lengths [20]. They are expressed at the bulk I-N phase transition $\xi_n^2=L/A_0(T_{IN}-T_*)$, $\xi_f^2=\mu_0 LS_0/\Delta\chi B^2$, $d_1=LS_0^2/W_1 S_0$, and $d_2=L/W_2$. The quantities G_i $(i=e,24,f,n)$ are dimensionless integrals depending on the nematic director field. In most cases their value is close one. We define them as

$$G_e=\frac{1}{V}\int\left(\frac{1}{2}(\vec\nabla\cdot\vec n)^2+\frac{K_{22}}{2K_{11}}(\vec n\times\vec\nabla\times\vec n)^2+\frac{K_{33}}{2K_{11}}(\vec n\cdot\vec\nabla\times\vec n)^2\right)d^3\vec x,$$

$$G_{24}=\frac{1}{V}\int\vec\nabla\cdot\left(\frac{\vec n\times\vec\nabla\times\vec n+\vec n\vec\nabla\cdot\vec n}{2}\right)d^3\vec x,$$

$$G_f=\frac{1}{V}\int\frac{(\vec n\cdot\vec e_f)^2}{2}\,d^3\vec x, \tag{7}$$

$$G_n=\frac{1}{V}\int\frac{3(\vec n\cdot\vec e)^2-1}{2}\,d^2\vec x,$$

$$V=\int d^3\vec x.$$

Here $d^3x=d^3r/R^3$. The contribution of point defects is given roughly by the term $t_{\rm def}\approx n_{\rm def}(\xi_n/R)^3$, where $n_{\rm def}$ is the number of defects per distance R. The dimensionless quantity G is related to the free energy via $G=(F/VRLS_0^2)(\xi_n/R)^2$. Note that the ratios K_{22}/K_{11} and K_{33}/K_{11} in Eq. (7) are not temperature dependent in this approximation.

The temperature dependence $s(t_n)$ is obtained via a minimization of Eq. (5). For $h_n^2<h_c^2=0.5$ the I-N transition is discontinuous, whereas it is gradual in the opposite case. In the discontinuous regime the phase transition takes place when [12] $t_n=1+h_n^2$, yielding an expression for the I-N phase-transition temperature $T_{IN}(R)$ within the cavity. The corresponding phase temperature shift $\Delta T_{IN}=T_{IN}-T_{IN}(R)$ is

$$\Delta T_{IN}=(T_{IN}-T_*)\left[\left(\frac{\xi_n}{R}\right)^2(-a_0 G_e^n+(a_1+a_2)G_{24})+\left(\frac{\xi_n}{\xi_f}\right)^2 G_f+\frac{\xi_n^2}{d_1 R}\,G_n-\frac{\xi_n^2}{d_2 R}-t_{\rm def}\right]. \tag{8}$$

For a typical LC the values of the material constants entering Eq. (8) are $T_{IN}-T_*\approx 1$ K, $\xi_n\approx 0.1\,\mu$m, and $a_i\approx 1$ $(i=0,1,2)$. For a surface with $W_i\approx 5\times10^{-5}$ J/m^2 $(i=1,2)$ and for $LS_0^2\approx 5\times10^{-12}$ J/m it follows that $d_i\approx 0.1\,\mu$m.

C. N–Sm-A phase transition

In the Sm-A phase we limit ourselves to the director fields that are compatible with the smectic layering. In the minimization procedure the order parameter η is first assumed to be spatially homogeneous. The resulting expression for the free energy is then minimized over η.

With this in mind the dimensionless free energy $G_{\rm Sm}=(F/VRC_\parallel\eta_0^2)(\xi_a/R)^2$ in the smectic phase is expressed as an expansion in $\varepsilon=\eta/\eta_0$:

$$G_{\rm Sm}=t_s\varepsilon^2+\varepsilon^4/2-h_s^2\varepsilon. \tag{9}$$

The effective smectic temperature t_s and the effective smectic external field h_s are given by

$$t_s=\frac{T-T_{NA}}{T_{NA}}+(q\xi_s)^2 G_e^s-\left(\frac{\xi_s}{d_{cp}}\right)^2, \tag{10a}$$

$$h_s^2=\frac{R}{d_p}\,G_s. \tag{10b}$$

The quantities in Eqs. (9) and (10) are defined as $\xi_s^2=C_\parallel/(\alpha_0 T_{NA})$, $d_0=C_\parallel\eta_0^2/W_{pa}\eta_0$, and $d_{cp}^2=C_\parallel/DS$ and G_e^s, G_s as

$$G_e^s=\frac{1}{V}\int\left((n\cdot\vec\nabla\Phi-1)^2+\frac{C_\perp}{C_\parallel}(\vec n\times\vec\nabla\Phi)^2\right)d^3\vec x,$$

$$G_s=\frac{1}{V}\int\cos[qR(\Phi-\Phi_s)]d^2\vec x. \tag{11}$$

The temperature dependence of ε is obtained via a minimization of Eq. (9). The N–Sm-A transition is gradual for $h_s>0$. For $h_s=0$ the transition is continuous and takes place at $t_s=0$. The corresponding temperature shift $\Delta T_{NA}=T_{NA}-T_{NA}(R)$, where $T_{NA}(R)$ denotes the N–Sm-A phase transition in the confined LC, is

$$\Delta T_{NA}=T_{NA}\left[-(q\xi_s)^2 G_e^s+\left(\frac{\xi_a}{d_{cp}}\right)^2\right]. \tag{12}$$

For a typical LC the value of ξ_s deeply in the Sm-A phase is comparable to the molecular size. It diverges at the continuous N–Sm-A phase transition. Characteristic values of the remaining typical distances in Eq. (12), to our knowledge, are not known.

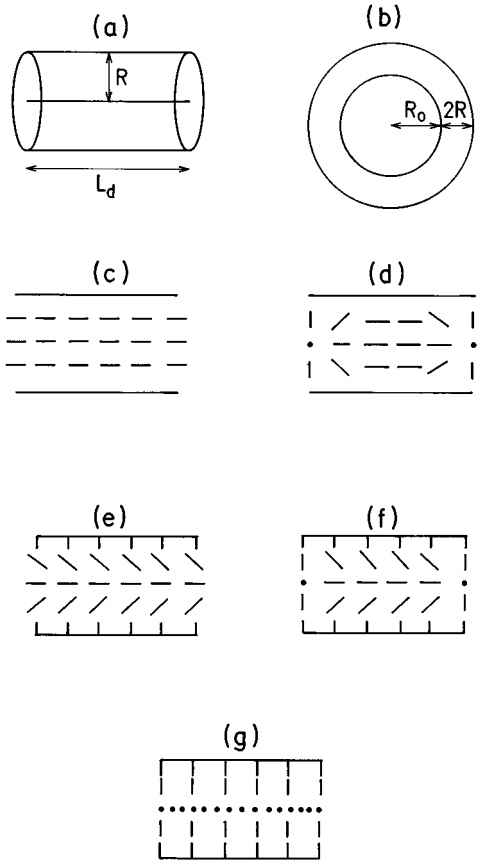

FIG. 5. Schematic presentation of model geometries simulating a typical cavity within a CPG sample. The cavity is described as (a) a cylinder of length L_d and radius R or (b) a space between two concentric cylinders of radii R_0 and R_0+2R, respectively. The corresponding director structures are (c) the homogeneous structure, (d) the homogeneous structure with point defects, (e) the escaped radial structure, (f) the escaped radial structure with point defects, and (g) the planar radial structure. For the geometry described in (b) the director field is either radially distributed (for the homeotropic anchoring) or perpendicular to this direction following the cylinders' curvature.

IV. MODEL STRUCTURES

Let us now discuss the phase behavior described in Sec. III with an emphasis on the R dependence. The phase temperature shifts given in Eqs. (8) and (12) are governed by explicit and implicit dependences on R. The latter is hidden in the integrals G_i $(i=e,24,n,f,\ldots)$. These in most cases weakly depend on R, e.g., G_i does not depend on R when $\mathbf{n}(\mathbf{r})$ scales with R.

To assess the values of G_i we need information about the director field. For this purpose we chose model structures that sufficiently well present the main characteristics of the real samples. In the first step we approximate the geometry of a characteristic cavity within the CPG sample by a cylinder of radius R and length L_d as shown in Fig. 5(a). Then we make predictions about possible director field structures within it. These are schematically shown in Figs. 5(c)–5(g). In general, the director field is dominantly determined by the surface condition if the anchoring is strong enough ($R/d_1 \gg 1$). We consider two extreme cases: *homeotropic* anchoring (the LC molecules tend to be aligned along the surface normal) and *planar* anchoring (the molecules are forced to lie in the limiting plane within which all directions are equivalent).

The planar anchoring case is modeled by the homogeneous (H) structure [Fig. 5(c)] or the homogeneous structure with point defects (HPD) [Fig. 5(d)]. In the H structure the director field is spatially homogeneous and points along the cylinder axis. In the HPD structure the domains with the director field similar to the H structure are separated by planes with the planar radial director profile.

In the case of homeotropic anchoring we choose as representatives the escaped radial [35] (ER) [Fig. 5(e)] or the escaped radial structure with point defects [35] (ERPD) [Fig. 5(c)]. In the ER structure **n** tends to be aligned along the surface normal at the cylinder surface. On approaching the center of the cylinder it gradually reorients along its axis. In the strong anchoring regime this structure is scale invariant. The ERPD structure consists of domains separated by planar radial planes with point defects. The director structure of each domain is similar to the ER structure, particularly in the limit $L_d \gg R$. Note that these structures can be realized if the anchoring is strong enough. This roughly corresponds to the regime [35,36] $R/d_1 > 1$. Below this regime the ER and ERPD structures tend to evolve into the topologically equivalent H structure.

The ER or H structures describe well the situation when the average distance between the closest cavity intersections within the CPG sample is large compared to R. At these intersections in general the director field cannot be matched without forming topological point defects. The point defect structures (HPD and ERPD) roughly simulate the case, where the average distance between two closest cavity intersections is L_d. Note that in an infinite long cylinder these two structures are not stable. The ERPD structure tends to evolve into the ER structure and HPD into the H structure.

In the case of strong homeotropic anchoring the ER and ERPD structures described above mimic well the ordering in the N phase not too close to the Sm-A phase [35,36]. Just above the $N-$Sm-A phase transition the bend nematic elastic constant is anomalously [20] increased due to pretransitional smectic order. Consequently, instead of the ER or ERPD structure, in which nematic bend elastic distortion is significant, the planar radial [35,36] director field [Fig. 5(g)] tends to form. In this structure the bend nematic deformation is absent and the director field radially streams from the center of the cylinder with a line defect along the cylinder axis.

Note that in studies treating the nematic structures within cylindrical cavities the planar polar (for homeotropic anchoring) and the planar bipolar structure (for planar anchoring) are often reported [35–37]. In these planar structures the director field is restricted to the plane with the normal along the cylinder axis. In both structures the director field is preferentially parallel in the central region of the cylinder tending to orient along the direction preferred by the anchoring interaction at the surface. In the case of strong anchoring these structures require two surface line defects running parallel to the cylinder axis. In the case of weak anchoring the free energy of these structures is similar to the free energy of the H structure. In the case of rather strong anchoring ($R/d_1 \gg 1$) these structures are not expected to be stable because of energetically costly line defects. In the weak an-

choring regime we also anticipate that the director field preferentially oriented along the approximate local symmetry axis of the void is closer to reality because of the spatial variation of the orientational axis.

The SEM photographs [6] of some CPG matrices reveal that their cylindrically shaped voids are relatively strongly curved. In order to estimate the influence of the curvature on the phase behavior we consider a LC confined between two concentric cylinders as shown in Fig. 5(b). The radius of the inner cylinder is R_0 and of the outer is R_0+2R. This configuration roughly mimics a curved cylindrical cavity of a radius R and curvature R_0. For the homeotropic anchoring we chose the radial distribution of the director field. In the planar case the director field is perpendicular to the radial direction. To test the behavior at the $N-$Sm-A transition we assume that in the Sm-A phase the layers grow from the surface in the case of homeotropic anchoring and are set perpendicular to the surface for the planar anchoring.

V. RESULTS AND DISCUSSION

Next we present results from the model. The expected temperature shifts of the I-N and $N-$Sm-A phase transition are analyzed in Secs. V A and V B, respectively. In Sec. V C theoretical findings are linked with our experimental results.

A. I-N phase transition

The I-N phase transition is gradual if $h_n^2>0.5$. As it is evident from Eq. (6b), this can happen if either K_{24}, W_1, or the external magnetic-field terms (or their combination) are strong enough. For $h_n^2<0.5$ the phase transition is discontinuous. The origins of the corresponding temperature shift are, according to Eq. (8), either the external magnetic field, elastic distortions, or surface interactions.

1. External field

We first analyze possible consequences of the external magnetic field. Its contribution to h_n and t_n is proportional to $G_f(\xi_n/\xi_f)^2$. The dependence on R enters only via G_f. In our experiment $\xi_f\approx 0.5\ \mu$m, thus $(\xi_n/\xi_f)^2\approx 0.04$. In the limit $R/\xi_f\gg 1$ all the molecules are oriented along the external field yielding the maximal value of $G_f=1$. In the opposite limit $(R/\xi_f=0)$ the randomly oriented cavities in the CPG samples imply that all directions of **n** are equally occupied yielding $G_s=\frac{1}{3}$. Therefore, in any case the value of G_f is of order one. The contribution of the magnetic field **B** to the temperature shift is expected to be $\Delta T_{IN}<0.04$ K and similarly the contribution to the effective field is $h_f^2<0.04$. Thus the external field contributions to t_n and h_n are in our case negligible.

2. Elastic distortions

To test the influence of the elastic distortions we study the model structures presented in Fig. 5. The character of the transition can be changed due to the linear contribution in S in the K_{24} term. Its contribution to h_n is proportional to $a_1G_{24}(\xi_n/R)^2$ [see Eq. (6b)]. Recent studies, suggest [35] that the value of the saddle splay elastic constant is close to that of the Frank elastic constants, i.e., one expects $a_1\approx 1$.

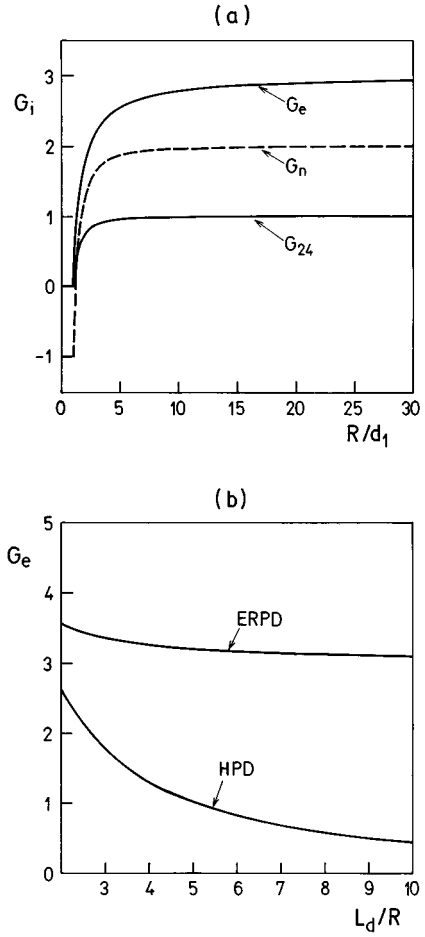

FIG. 6. Integrals G_i entering Eqs. (7) as a function of R. (a) $G_e=G_c(R/d_1)$, $G_{24}=G_{24}(R/d_1)$, and $G_n=G_n(R/d_1)$ for the ER structure and (b) $G_c=G_e(L_d/R)$ for the HPD and ERPD structures.

For the ER and the ERPD structure in the strong anchoring regime G_{24} is of order one. This is evident from Fig. 6(a), where the dependence of integrals G_i $(i=e,24,n)$ on R/d_1 is shown in the approximation of equal elastic constants $(K\equiv K_{24}=K_{11}=K_{33})$. In contrast, for the H structure $G_{24}=0$ and for the HPD structure it is much less than in the ER or ERPD structure in the regime of interest. Therefore, this term can change the character of the transition only in the case of strong enough homeotropic anchoring (that is, $RW_1/K=R/d_1>1$) if in addition $R/\xi_n\approx 1$. Assuming $R\approx\xi_n\approx 0.1\ \mu$m, $K\approx 5\times 10^{-12}$ J/m, which suggests that anchoring must be larger than $W_1\approx 5\times 10^{-5}$ J/m^2, which represents a sensible value for the samples studied.

In the case that $h_n^2<0.5$ the temperature shift [Eq. (8)] of the I-N transition is of interest. For a typical LC $a_i\approx 1$ $(i=0,1,2)$. The values of G_i $(i=e,24)$ are of order one for the ER and ERPD structures and are almost independent of R in the strong anchoring regime. Therefore, in this regime the phase temperature shift due to the elastic distortion is expected to scale with cavity size as $1/R^2$. In the very weak anchoring regime, on the other hand, all G_i are zero for the both structures. The variation of G_i when going from the very weak anchoring to the strong anchoring regime for equal elastic constants is demonstrated on the ER structure in Fig. 6(a). We see that G_i saturates at a constant value already

when $R/d_1 \approx 5$. The weak anchoring regime, where surface and elastic interactions are comparable, lies between $R/d_1 \approx 5$ and $R/d_1 = 1$. Consequently, G_i strongly varies with R. The very weak anchoring regime is below the critical value [35,36] $R/d_1 = 1$. For $W_1 = 5 \times 10^{-5}$ J/m^2 the weak anchoring regime lies between radii $R \approx 0.5$ and 0.1 μm. For the H structure $G_e = G_{24} = 0$ and for the HPD structure these integrals tend to zero if defects are not too close in comparison to R. A dependence of G_e on the ratio L_d/R for the ERPD and HPD structures is shown in Fig. 6(b).

We thus find that the temperature shifts of order 1 K or a change of the character of the I-N transition due to elastic terms are expected only (i) for the homeotropic anchoring, which (ii) must be strong enough, and (iii) $R/\xi_n \approx 1$. From (ii) and (iii) it follows that conditions $W_1 > 5 \times 10^{-5}$ J/m^2 and $R \approx 0.1$ μm must be realized.

In these calculations the effect of curvature is not taken into account. To asses its influence on the nematic growth we consider the geometry presented in Fig. 5(b). For the homeotropic anchoring the director structure between concentric plates is assumed to be radial and tangential in the case of planar anchoring. Both these structures give the same contribution to the nematic elastic term if $K_{11} = K_{33}$. Taking these structures into account and neglecting other contributions, we get the expression for G [Eq. (5)] with $h_n = 0$ and

$$t_n = \frac{T - T_*}{T_{IN} - T_*} + \frac{a_0 \xi_n^2}{4RR_0} \frac{\ln(1 + 2R/R_0)}{1 + R/R_0}. \tag{13}$$

The corresponding temperature variation of the order parameter is then

$$S(T) = S_0 \frac{3 + \sqrt{9 - 8t_n}}{4}. \tag{14}$$

In our samples the condition $R/R_0 \ll 1$ is fulfilled. Consequently, to a good approximation the corresponding temperature shift can be expressed as $\Delta T \approx (T_{IN} - T_*) a_0 \xi_n^2 / 2R_0^2$. We see that the effect of curvature becomes significant when $R_0 \approx \xi_n$. For cases $R > \xi_n$ and $R \ll R_0$ the temperature shift of the I-N phase transition due to the curvature is negligible. Note that in our samples the curvature of voids is randomly varying. To simulate this we average Eq. (14) over different R_0 distributed according to the Gaussian distribution $P(R_0) = 2/(\sigma\sqrt{\pi}) \exp[-(R_0 - R_m)^2/\sigma^2]$, where $\sigma = \Delta R/2 \ln 2$. Here R_m corresponds to the average curvature of the sample and ΔR is the width of the Gaussian distribution. The corresponding averaged nematic ordering is designated $\langle S \rangle$. In Fig. 7 we show the temperature dependence of $\langle S \rangle$ for $R = 0.2$, 0.025, 0.012, and 0.0035 μm. The mean curvature of the system is set to $R_m = 5R$ and $\Delta R = R_m$. For $R = 0.2$ μm the $\langle S \rangle$ dependence follows almost exactly the bulk behavior. In contrast, if $R < \xi_n$ the curvature variations play an important role. The corresponding temperature evolution seems to be gradual, although in this calculation it consists of a superposition of discontinuous contributions.

3. Surface contribution

The surface term linear in S can change the character of the I-N transition as it is evident from Eq. (6b). Its contribution to h_n is proportional to $G_n \xi_n^2 / R d_1$. It scales as $1/R$ in the strong anchoring regime. In the weak anchoring case the dependence can be more complicated depending on the variation of G_n with R as shown in Fig. 6(a) for the case of the ER structure in the approximation of equal nematic elastic constants ($K_{24} = K_{11} = K_{33}$). The weak anchoring regime is roughly given by $R/d_1 < 5$. The value of G_n is in the whole regime of order one. Therefore, a change of the transition is expected when $\xi_n^2/Rd_1 \approx 1$. For $W_1 \approx 5 \times 10^{-5}$ J/m^2 the critical value of R is around 0.1 μm.

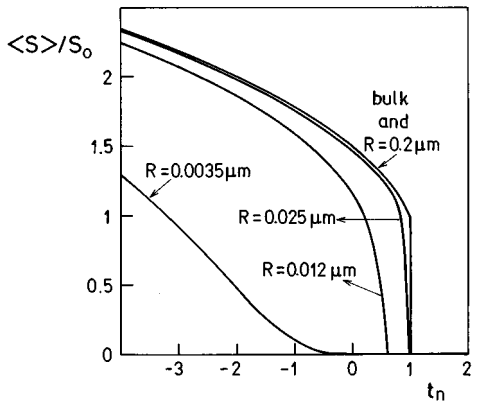

FIG. 7. Influence of the curvature on the temperature dependence of the nematic orientational order parameter. The cases $R = 0.2$, 0.025, 0.012, and 0.0035 μm are shown for the mean curvature $R_m = 10R$ and $\delta R = R_m/2$. For $R = 0.2$ μm the curves are indistinguishable from the bulk dependence.

In contrast, both the linear and the quadratic term contribute to the phase temperature shift if $h_n^2 < 0.5$. The linear term increases ΔT_{IN} while the square term decreases it. The shift of either contribution can be of order 1 K if $\xi_n^2/Rd_1 \approx 1$. However, in the case of the linear term the change of the character of the transition will take place before such a shift is realized in view of a similar contribution of this term to h_n and ΔT_{IN}.

B. N–Sm-A phase transition

1. Elastic distortions

We consider the case where the surface positional anchoring term plays a negligible role so that the N–Sm-A phase transition is of second order. We first approximate the geometry of an average CPG cavity by a cylindrical segment. At the N–Sm-A phase transition for the planar anchoring orientational distribution the director field is homogeneous and planar radial for the homeotropic anchoring. Both director profiles are compatible with Sm-A layers yielding, within our model, $G_c^s = 0$ if the concentration of defects in $\mathbf{n}$ is negligible. If defects are present the Sm-A layer structure is locally destroyed. The size of the perturbed region in the Sm-A ordering at the transition is given by the typical cavity size. This is because the bulk N–Sm-A phase transition is of the second order and consequently the bulk smectic correlation length $\xi_s(T)$ diverges.

In addition to defects, the curvature also plays an important role in the smectic growth for all matrices studied. According to our estimates, this effect overwhelms the effect of

defects provided the average distance between adjacent defects is much larger than R. In contrast, the nematic ordering is substantially affected by the curvature only for matrices with $R \ll \xi_n$ (see Fig. 7). To demonstrate the influence of the curvature on the smectic growth we consider the geometry given in Fig. 5(b) for the planar anchoring. The smectic layers run perpendicular to the cylindrical surface. In calculations we assume that the layers are nondistorted at the outer cylinder where the relative number of LC molecules is maximal. Because of the curvature R_0, the compression of layers continuously increases on approaching the inner cylinder. With this in mind and neglecting the surface interaction terms ($h_s=0$), we find the expression for G_{Sm} [Eq. (9)] with

$$t_S=\frac{T-T_{NA}}{T_{NA}} + (q\xi_s)^2\,\frac{\frac{3}{2}+\frac{4R}{R_0}+\frac{1}{2}\left(1+\frac{2R}{R_0}\right)^2\left[-3+2\ln\left(1+\frac{2R}{R_0}\right)\right]}{\frac{2R}{R_0}\left(1+\frac{R}{R_0}\right)}. \tag{15}$$

For $R/R_0 \ll 1$ the corresponding temperature shift for a given curvature R_0 is $\Delta T_{NA}(R_0)\approx T_{NA}\xi_s^2 q^2 R^2/R_0^2$. Typically $\xi_s^2 q^2 \approx 1$ and $R/R_0 \approx \frac{1}{10}$, giving rise to the temperature shifts of order 1 K for any R. To get a more realistic result we average η over different values of R_0 distributed according to the Gaussian distribution $P(R_0)=2/(\sigma\sqrt{\pi})\exp[-(R-R_m)^2/\sigma^2]$ for given T and R. The corresponding temperature dependence of the averaged smectic ordering $\langle\eta\rangle$ is shown in Fig. 8(a) for $R=0.2$ μm and two different average curvatures ($R_m=5R$ and $10R$). We see that in both cases the depression of the smectic ordering is prominent in contrast to the nematic case. The suppressed Sm-A ordering is in our experiment observed indirectly via its influence on the nematic ordering. To illustrate this coupling effect we calculate the temperature evolution of the nematic order, taking into account the coupling between the nematic and smectic order parameters [the term with the coupling constant D in Eq. (2)]. This dependence is shown in Fig. 8(b). The $\langle S\rangle$ dependence obtained from the averaging procedure described above is compared to the bulk one. The bulk ordering was obtained via minimization of the dimensionless total free energy

$$G_{\mathrm{tot}}=t_n s^2-2s^3+s^4+\left(\frac{\xi_n}{\xi_s}\right)^2\left(\frac{C_\parallel \eta_0^2}{LS_0^2}\right) \times\left[t_s\varepsilon^2+\frac{\varepsilon^4}{2}-\left(\frac{\xi_s}{d_{cp}}\right)^2\varepsilon^2 s\right]. \tag{16}$$

Here $G_{\mathrm{tot}}=F(\xi_n/R)^2/VRLS_0^2$ and the surface contributions in Eq. (2) are discarded. In a similar way the smectic ordering in the curved cavity was obtained by introducing an additional elastic term that just rescales the parameter t_s [see Eq. (15)]. The ordering was then averaged over different curvatures as already described above. The dependence in Fig. 8(b) corresponds to $T_{IN}-T_{AN}=10$ K, $(\xi_n/\xi_s)^2(C_\parallel\eta_0^2)/LS_0^2=10^6$, and $(\xi_s/d_{cp})^2=0.004$. Note that the N–Sm-A phase transition is shifted for 3 K above T_{NA} due to the coupling term. The onset of the Sm-A ordering is clearly manifested in bulk via the anomaly observed in the temperature dependence of S. For the suppressed Sm-A ordering shown in Fig. 8(a) this sharp anomaly consequently disappears.

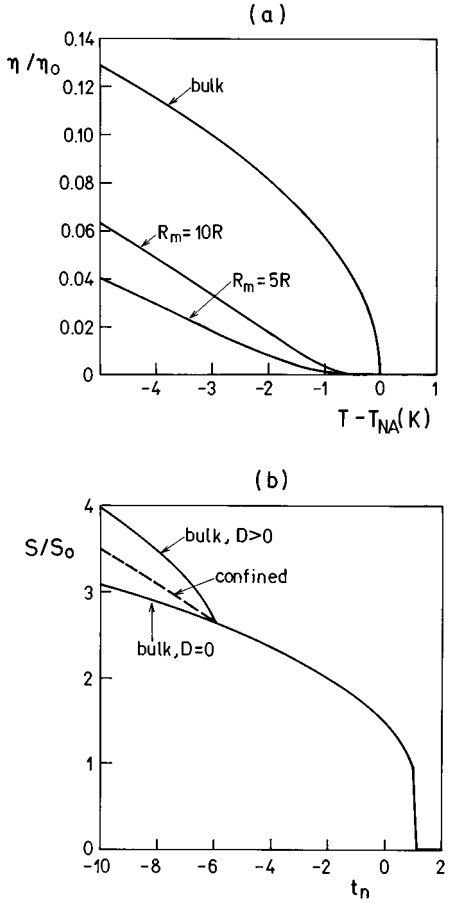

FIG. 8. (a) Temperature evolution of the smectic order parameter for $R_m=5R$ and $10R$, $\Delta R=R_m/2$, and $R=0.2$ μm. (b) Calculated nematic order parameter coupled with the smectic ordering. Full line, bulk; full line and dashed part, CPG matrix. In the 8 CB LC a unit in the t_n scale roughly corresponds to 1 K.

On the other hand, in the case of homeotropic anchoring the depression of the Sm-A ordering due to the curvature is not so effective. For such a structure the splay nematic distortion is dominant. In this case $G_c^s=0$ within our model. In reality, the bending of smectic layers gives rise to elastic distortions in the smectic order. To take this into account higher-order terms [24] are needed in Eq. (2), yielding second-order derivatives in Φ.

2. Surface contribution

A smooth surface in general enhances the degree of nematic ordering. Indirectly also the smectic ordering is stimulated particularly for the case of homeotropic anchoring. In this case the pretransitional smectic ordering initiated from the surface is expected. The surface support for the smectic ordering is less pronounced in the planar case where smectic layers are set perpendicular to the surface.

C. Discussion of experimental results

We first try to extract from the experimental results the anchoring conditions and the corresponding anchoring strengths. The nontreated CPG surface is smooth [6] down to the nanometer scale and is consequently believed to enforce the planar anchoring. This assumption is based on results obtained from surfaces with similar properties [32]. On the other hand, the silane treated surface is known to enforce the homeotropic anchoring. In a cylindrical geometry this anchoring condition orients molecules along its direction only if the condition $RW_1/K>1$ is realized, with K standing for an average nematic elastic constant. For $R=0.2\ \mu$m, $K\approx10^{-12}$ J/m. This condition implies that $W_1>2.5\times10^{-5}$ J/m^2.

The anchoring strength can be assessed from the results presented in Fig. 3. The line shape of the absorption spectra is shown as a function of the reorientation angle θ_f for $R=0.2\ \mu$m CPG samples. The measured spectra suggest that the director structure to a great extent followed the reorientation of the field **B** in both treated and nontreated cases. In the nontreated sample for $\theta_f=0$ the pronounced external wings in $I(\nu)$ reveal preferential director field alignment along **B**. The external field is in this case strong enough to break the global isotropic director field distribution imposed by the CPG matrix. The claim that **n** follows the reorientation of the sample is based on the fact that the separation of pronounced wings in $I(\nu)$ is roughly proportional to $(3\cos^2\theta_f-1)/2$. In contrast, in the nontreated sample the overall isotropic **n** distribution is only weakly perturbed by the external magnetic field. Consequently, the influence of θ_f on **n** is weak.

This indicates that the CPG matrix locked in the director structure after it was established on cooling from the isotropic phase. Therefore, the orientational anchoring strength W_1 is relatively strong in comparison to the external field. To assess its value we assume a constant director field across the cavity. The external field and the easy axis are set at a finite angle to enforce the competition. The relative weights of the surface and the external field contribution in F are given by R/d_1 and $(R/\xi_f)^2$, respectively. The surface influence is dominant if $R/d_1\gg(R/\xi_f)^2$. In our experiment $\xi_f\approx0.5\ \mu$m, suggesting $W_1\gg5\times10^{-6}$ J/m^2. Therefore, we anticipate that in both treated and nontreated samples the anchoring strength is larger than $W_1=10^{-5}$ J/m^2.

Shapes of the measured absorption spectra are consistent with the belief that in the silane-treated samples the anchoring is homeotropic and in the nontreated samples planar. For homeotropic anchoring the surface locally supports only one direction compared to several allowed directions in the planar case. For this reason, in the nontreated case the director field has more opportunities to match the tendencies of the surface anchoring and the external magnetic field, which are in general in competition. Consequently, $I(\nu)$ is more affected by the external magnetic field in the nontreated case. Note that in the case of homeotropic anchoring we assume that W_1 is large enough (i.e., $RW_1/K>1$) to enforce its tendency to **n**. For $R=0.2\ \mu$m and $K\approx10^{-12}$ J/m this implies that $W_1>2.5\times10^{-5}$ J/m^2, in accordance with estimates made in the previous paragraphs.

We next consider possible origins of the I-N phase temperature shifts measured in the nontreated CPG matrices filled with 5CB LCs. The results indicate that down to $R=0.025\ \mu$m the I-N transition remains discontinuous and ΔT_{IN} is below 1 K. According to the previous discussion in these samples the anchoring is planar. In this case elastic distortions are expected to be relatively weak if the concentration of defects is not too high. The observed phase temperature shift is most probably dominated by the surface term originating from the incomplete coupling among LC molecules at the LC-CPG interface, suggesting the scaling $\Delta T_{IN}\propto1/R$. Our measurements yield $\Delta T_{IN}\propto1/R^{1.3\pm0.3}$, supporting this belief. Relative small temperatures shifts indicates that d_1 and d_2 in Eq. (8) are comparable and $d_1>d_2$. Note that the expression (8) for ΔT_{IN} is not expected to give accurate quantitative estimates for CPG samples with $R<\xi_n(T_{IN})\approx0.1\ \mu$m. In this regime $S(\mathbf{r})$ variations are in general substantial and probably coupled to $\mathbf{n}(\mathbf{r})$, which is discarded in our model.

The samples characterized by $R=3.5$ and 12 nm exhibit a gradual evolution of the nematic growth. In our model this requires $h_n^2>0.5$ and according to Eq. (6b) can be attributed only to the surface interaction if the curvature of voids plays a negligible role. In such a case the previously assessed value $W_1>10^{-5}$ J/m^2 yields $h_n>1$ for these samples. In such narrow cavities a noncritical character of the surface interactions in the temperature regime studied prevails over the bulk tendency of the LC resulting in the gradual nematic growth. The K_{24} contribution to h_n is expected to be negligible because of weak elastic distortions enabled by the planar anchoring condition. However, in such small cavities the ordering is very susceptible to various perturbations such as variations in curvature and defects at cavity intersections. They introduce a kind of random field [17,19] that can also change the character of the transition. Also we can not exclude the possibility, demonstrated in Fig. 7, that the observed gradual evolution is in fact a superposition of domain contributions with different degrees of nematic ordering. Within each of them the I-N transition remains discontinuous. A domain is designated as a LC region between adjacent cavity interconnections. The calculations indicate that the curvature begins to play an important role just in the regime where the gradual onset of nematic ordering was observed.

The belief that in the silane-treated sample the anchoring is homeotropic is also supported by measurements across the bulk $N-$Sm-A transition in 8CB confined to the $R=0.2\ \mu$m sample. Our calculations on model systems [Fig. 5(b)] suggest that if the planar anchoring is realized the Sm-A ordering is efficiently suppressed by the curvature of cylindrically shaped cavities. Spatial variations in the degree of Sm-A ordering are expected to be substantial because the curvature of cavities varies relatively strongly within the CPG matrix. In the case of homeotropic anchoring the influence of the curvature is far less effective. In the silane-treated sample the experiment shows that the smectic ordering closely follows the bulk temperature behavior. Thus the smectic ordering is in this case weakly affected by the confinement, which, according to our estimates can be realized only for homeotropic anchoring. In the nontreated sample the experimental results are too scattered to make definite conclusions.

VI. CONCLUSIONS

The deuteron NMR absorption spectra of 5CB and 8CB liquid crystals immersed in various CPG matrices were measured. For the 5CB LC the character and the temperature shift of the *I*-*N* phase transition were studied as a function of R in the nontreated CPG cavities exhibiting a planar anchoring condition. For $R \geq 0.025$ μm the *I*-*N* phase transition is discontinuous and the corresponding phase temperature shift scales as $\Delta T_{IN} \propto 1/R^{1.3\pm0.3}$. Within our model the observed decrease of the phase transition temperature is mainly attributed to the S^2 term in the surface free energy, which scales as $1/R$. This is in fact the finite-size effect because this term is believed to appear due to incomplete interaction [31,32] of LC molecules at the LC-CPG interface. Our measurements indicate that in CPG samples with $R = 3.5$ and 12 nm, the transition seems to be gradual. Within our model a possible origin for this effect is the W_1 contribution or the random curvature of voids. In such small cavities the degree of ordering becomes increasingly sensitive to details in a void with decreased R. In our theoretical treatment we express ΔT_{IN} as a function of the various contributions neglecting the effect of randomness. Rough estimates on a model system indicate that in the CPG samples the effect of randomness becomes important for $R < \xi_n$. In this regime the main origin of randomness is noncorrelated curvatures of cylindrical voids.

It is interesting to compare the phase-transition temperature shifts in CPG matrices with those obtained in aerogels where randomness is expected to play a dominant role. The relevant size characterizing an aerogel matrix is the mean free path L in the empty regions. The experimental results [38] by Wu *et al.* suggest that ΔT_{IN} scales as $1/L$. They claim that the observed scaling is dominantly determined by randomness and not by surface or finite-size effects. However, a Monte Carlo study performed by Bellini *et al.* [39] suggests that the resulting temperature shift emerges from a rather complicated coupling between the surface phenomena and randomness.

We further studied the effect of surface treatment on the phase behavior of the 8CB LC confined in the CPG sample characterized by $R = 0.2$ μm. The silane-treated surface exhibits homeotropic anchoring and the nontreated surface planar anchoring. In both cases the anchoring strength is estimated to be larger than 10^{-5} J/m^2. The theoretical analysis indicates that the $N-$Sm-*A* transition is substantially more affected by the curvature of voids than the *I*-*N* transition for the planar anchoring condition. Experimental data are in accordance with this prediction. In the nontreated sample the degree of Sm-*A* ordering is expected to be strongly space dependent because of a pronounced variation in the curvature of cavities of the CPG matrix. This results in a more gradual evolution of the Sm-*A* ordering compared to the bulk sample. In contrast, in the silane-treated sample the Sm-*A* ordering is only weakly perturbed.

It is reasonable to relate our results on the effect of confinement on the Sm-*A* growth to those obtained in Anopores and aerogels. These samples represent the extreme limits of a CPG geometry. The Anopore matrix simulates the case of a CPG sample if interconnectedness and curvature of CPG voids have negligible role. The other extreme corresponds to the aerogel matrix.

Iannacchione and Finotello studied [2] 8CB LCs confined to Anopores of radius $R = 0.1$ μm. The surface was either lecithin treated, enforcing homeotropic anchoring, or nontreated, resulting in a planar anchoring condition. In both cases the $N-$Sm-*A* phase transition was substantially affected by confinement, particularly in the case of nontreated surface. The rough nontreated surface inhibited the smectic growth, which was consequently initiated from the central region of the cylinders. On the other hand, in the case of homeotropic anchoring the smectic layers were initiated at the surface.

Experiments performed on aerogels reveal that the Sm-*A* growth is also strongly suppressed. It is believed that randomness [38] is responsible for that. The location where smectic layers begin to grow strongly depends on the type [20,40] of Sm-*A* LC characterized by the ratio between the smectic correlation length ξ_s and smectic penetration length λ. For type-I Sm-*A* LCs ($\xi_s/\lambda < 1$) it begins to grow in the central region of voids, whereas for type-II Sm-*A* LCs ($\xi_s/\lambda > 1$) it starts to grow from the surface.

In contrast, our results obtained with the silane-treated surface suggest a weak influence on the smectic growth. This discrepancy in the behavior is most probably due to a larger typical void size of the CPG sample studied and in particular to the smooth surface supporting the smectic growth. Namely, the smooth surface exhibiting homeotropic anchoring is known to support smectic growth. Results obtained by Aliev and Breganov [15] demonstrate this effect. They have reported surface-induced smectic ordering within a porous matrix even in the case of a 5CB liquid crystal, which in bulk does not exhibit a smectic phase.

It should be stressed that deuteron NMR measurements are far from being ideal in probing the smectic layer configuration. The smectic order is in this case assessed indirectly via its influence on nematic ordering. A method directly coupled to smectic layers (e.g., x-ray scattering) would be of interest to reveal more details about the onset of smectic ordering in CPG samples.

ACKNOWLEDGMENTS

We gratefully acknowledge the financial support of the Slovenian Ministry of Science and Technology (Grant No. J1-7067) and the Copernicus Project (No. IC15-CT96-0744).

[1] *Liquid Crystals in Complex Geometries Formed by Polymer and Porous Networks*, edited by G. P. Crawford and S. Žumer (Taylor and Francis, London, 1996).

[2] G. S. Iannacchione and D. Finotello, Phys. Rev. E **50**, 4780 (1994).

[3] G. S. Iannacchione, J. T. Mang, S. Kumar, and D. Finotello, Phys. Rev. Lett. **73**, 2708 (1994).

[4] R. O. Crawford, G. P. Crawford, J. W. Doane, S. Žumer, M. Vilfan, and I. Vilfan, Phys. Rev. E **48**, 1998 (1993).

[5] M. D. Dadmun and M. Muthukumar, J. Chem. Phys. **98**, 4850 (1993).
[6] S. Kralj, A. Zidanšek, G. Lahajnar, I. Muševič, S. Žumer, R. Blinc, and M. M. Pintar, Phys. Rev. E **53**, 3629 (1996).
[7] Ch. Cramer, Th. Cramer, F. Kremer, and R. Stannarius, J. Chem. Phys. **106**, 3730 (1997).
[8] G. S. Iannacchione, G. P. Crawford, S. Žumer, J. W. Doane, and D. Finotello, Phys. Rev. Lett. **71**, 2595 (1993).
[9] S. Tripathy, C. Rosenblatt, and F. M. Aliev, Phys. Rev. Lett. **72**, 2725 (1994).
[10] N. A. Clark, T. Bellini, R. M. Malzbender, B. N. Thomas, A. G. Rappaport, C. D. Muzny, D. W. Schaefer, and L. Hrubesh, Phys. Rev. Lett. **71**, 3505 (1993).
[11] G. Schwalb and F. W. Deeg, Phys. Rev. Lett. **74**, 1383 (1995).
[12] A. Zidanšek, S. Kralj, G. Lahajnar, and R. Blinc, Phys. Rev. E **51**, 3332 (1995).
[13] A. Mertelj and M. Čopič, Phys. Rev. E **55**, 504 (1997).
[14] F. M. Aliev, Kristallografiya **33**, 969 (1988) [Sov. Phys. Crystallogr. **33**, 573 (1988)].
[15] F. M. Aliev and M. N. Breganov, Zh. Eksp. Teor. Fiz. **95**, 122 (1889) [Sov. Phys. JETP **68**, 70 (1989)].
[16] M. Dadmun and M. Muthukumar, J. Chem. Phys. **97**, 578 (1992).
[17] A. Maritan, M. Ciepak, T. Bellini, and R. Banavar, Phys. Rev. Lett. **72**, 4113 (1994).
[18] K. Uzelac, A. Hasmy, and R. Jullien, Phys. Rev. Lett. **74**, 422 (1995).
[19] D. J. Cleaver, S. Kralj, T. J. Sluckin, and M. P. Allen, in *Liquid Crystals in Complex Geometries Formed by Polymer and Porous Networks* (Ref. [1]), p. 467.
[20] P. G. de Gennes and J. Prost, *The Physics of Liquid Crystals* (Oxford University Press, Oxford, 1993).
[21] A. Abragam, *The Principles of Nuclear Magnetism* (Clarendon, Oxford, 1962).
[22] S. Žumer, S. Kralj, and M. Vilfan, J. Chem. Phys. **91**, 6411 (1989).
[23] E. B. Priestley, P. J. Wojtowitz, and P. Sheng, *Introduction to Liquid Crystals* (Plenum, New York, 1974), p. 143.
[24] S. R. Renn and T. C. Lubensky, Phys. Rev. A **38**, 2132 (1988).
[25] S. Kralj and S. Žumer, Phys. Rev. E **54**, 1610 (1996).
[26] D. W. Allender, G. P. Crawford, and J. W. Doane, Phys. Rev. Lett. **67**, 1442 (1991).
[27] V. M. Pergamenshchik, Phys. Rev. E **47**, 1881 (1993).
[28] V. M. Pergamenshchik, Phys. Rev. E **48**, 1254 (1993).
[29] G. Barbero and A. Strigazzi, J. Phys. (France) Lett. **45**, 857 (1984).
[30] M. Nobili and G. Duran, Phys. Rev. A **46**, R6174 (1992).
[31] Poniewierski and T. J. Sluckin, Liq. Cryst. **2**, 281 (1987).
[32] G. Barbero, E. Miraldi, and A. Stepanescu, J. Appl. Phys. **68**, 2063 (1990).
[33] T. J. Sluckin (private communication).
[34] A. I. Alexe-Ionescu, G. Barbero, and G. Durand, J. Phys. II **3**, 1247 (1993).
[35] G. P. Crawford, D. W. Allender, and J. W. Doane, Phys. Rev. A **45**, 8693 (1992).
[36] S. Kralj and S. Žumer, Phys. Rev. E **51**, 366 (1995).
[37] R. J. Ondris-Crawford, M. Ambrožič, J. W. Doane, and S. Žumer, Phys. Rev. E **50**, 4773 (1994).
[38] L. Wu, B. Zhou, C. W. Garland, T. Bellini, and D. W. Schaefer, Phys. Rev. E **51**, 2157 (1995).
[39] T. Bellini, N. A. Clark, C. D. Muzny, L. Wu, C. W. Garland, D. W. Schaefer, and B. J. Oliver, Phys. Rev. Lett. **69**, 788 (1992).
[40] T. Bellini, C. Chiccoli, P. Pasini, and C. Zannoni, Phys. Rev. E **54**, 2647 (1996).